Net primary production of terrestrial ecosystems in China and its equilibrium responses to changes in climate and atmospheric CO_2 concentration

X. Xiao[1,2], J.M. Melillo[1], D.W. Kicklighter[1], Y. Pan[1], A.D. McGuire[3] and J. Helfrich[1]

[1]The Ecosystems Center, Marine Biological Laboratory, Woods Hole, MA 02543
[2]The Joint Program on the Science and Policy of Global Change,
Massachusetts Institute of Technology, Cambridge, MA 02139
[3]Institute of Arctic Biology, University of Alaska, Fairbanks, AK 99775

Abstract

We used the Terrestrial Ecosystem Model (TEM, version 4.0) to estimate net primary production (NPP) in China for contemporary climate and NPP responses to elevated CO_2 and climate changes projected by three atmospheric general circulation models (GCMs): Goddard Institute for Space Studies (GISS), Geophysical Fluid Dynamic Laboratory (GFDL) and Oregon State University (OSU). For contemporary climate at 312.5 ppmv CO_2, TEM estimates that China has an annual NPP of 3,653 TgC yr^{-1} (10^{12} gC yr^{-1}). Temperate broadleaf evergreen forest is the most productive biome and accounts for the largest portion of annual NPP in China. The spatial pattern of NPP is closely correlated to the spatial distributions of precipitation and temperature.

Annual NPP of China is sensitive to changes in CO_2 and climate. At the continental scale, annual NPP of China increases by 6.0% (219 TgC yr^{-1}) for elevated CO_2 only (519 ppmv CO_2). For climate change with no change in CO_2, the response of annual NPP ranges from a decrease of 1.5% (54.8 TgC yr^{-1}) for the GISS climate to an increase of 8.4% (306.9 TgC yr^{-1}) for the GFDL-q climate. For climate change at 519 ppmv CO_2, annual NPP of China increases substantially, ranging from 18.7% (683 TgC yr^{-1}) for the GISS climate to 23.3% (851 TgC yr^{-1}) for the GFDL-q climate. Spatially, the responses of annual NPP to changes in climate and CO_2 vary considerably within a GCM climate. Differences among the three GCM climates used in the study cause large differences in the geographical distribution of NPP responses to projected climate changes. The interaction between elevated CO_2 and climate change plays an important role in the overall response of NPP to climate change at 519 ppmv CO_2.

Submitted to: *Acta Phytoecologica Sinica* (published in China)
Author responsible for correspondence: Dr. Xiangming Xiao, The Ecosystems Center, Marine Biological Laboratory, Woods Hole, MA 02543, Tel: (508)289-7498, Fax: (508)457-1548, Email: xiao@lupine.mbl.edu
Key words: spatial patterns, climate models, ecosystem models, impact assessment

1. Introduction

Atmospheric concentrations of CO_2 and other long-lived greenhouse gases (e.g., N_2O) will continue to increase in the next century as the result of increasing anthropogenic emissions of these trace gases. Increasing greenhouse gases will further increase the radiative forcing of climate. For doubled CO_2, a number of atmospheric general circulation models (GCMs) estimate that globally averaged surface air temperature will increase in the range of 1.5 ˚C to 4.5 ˚C (Mitchell, *et al.*, 1990). Globally, there are also large geographical variations in the changes of precipitation and clouds projected by GCMs. The increasing atmospheric CO_2 concentration and resultant climate change are likely to have significant impacts on net primary production of terrestrial ecosystems (Melillo, *et al.*, 1990). Net primary production of terrestrial ecosystems is important in estimating land carrying capacity, which is critically relevant to the social and economic development of a country like China. China has a very large human population (about $1/5$ of the world population) and limited natural resources, especially fertile lands. The total land area in China is only about $1/15$ of the world land area and about 65% of this area is hills, mountains and plateau (Xiong and Li, 1988).

In China, the magnitude and spatial patterns of temperature and precipitation will change significantly according to simulations of a GCM for a doubling of atmospheric CO_2 concentration (Zhang and Wang, 1993; Wang and Zhang, 1993). Few studies have examined impacts of climate change on net primary production (NPP) of natural ecosystems in China (Zhang, 1993; Xiao, *et al.*, 1995). Zhang (1993) applied a regression model (Chikugo model, Uchijima and Seino, 1985), which uses annual values of climate variables (*e.g.*, temperature, precipitation, relative humidity) to estimate NPP of various ecosystems in China for contemporary climate. Zhang (1993) also calculated the responses of NPP to: (1) +2 ˚C and 20% increase of annual precipitation, and (2) +4 ˚C and 20% increase of annual precipitation in China. Net primary production increases for all the vegetation types under these climate change conditions (Zhang, 1993). However, the Chikugo model is basically a regression model based on correlation between NPP and climate, and the model has not considered the possible limitations of nutrient availability (*e.g.*, nitrogen) on NPP. Generally, the potential of application of regression models for future projection is limited because the regressions may not be appropriate for climatic conditions that are novel to terrestrial ecosystems (Melillo, *et al.*, 1993).

Recently, a number of processed-based ecosystem models, which are integrated with geographically referenced spatial data, have been applied to estimate responses of NPP and carbon storage to changes in climate and atmospheric CO_2 concentration at the global scale (Melillo, *et al.*, 1993; McGuire, *et al.*, 1995, 1996; Xiao, *et al.*, 1996a) and the continental scale, *e.g.*, South America (Raich, *et al.*, 1991), North America (McGuire, *et al.*, 1992, 1993) and conterminous United States (VEMAP Members, 1995). Estimates of NPP responses vary among the GCMs used in the studies across the scales of grid cell, biome, continent and the globe (Melillo, *et al.*, 1993; VEMAP, 1995; Xiao, *et al.*, 1996a). The process-based ecosystem models integrate key ecosystem processes such as plant photosynthesis, plant respiration, decomposition of soil organic

matter and nutrient cycling, which interactively affect NPP. These ecological processes are controlled by a number of abiotic factors, *e.g.*, water, light, temperature, soil texture and nutrients. The simultaneous interactions among the dynamics of carbon, nitrogen and water are complex and spatially variable.

In this study, we used a process-based global terrestrial biogeochemistry model, the Terrestrial Ecosystem Model (Raich, *et al.,* 1991; McGuire, *et al.,* 1995, 1996). First, we applied TEM to estimate the magnitude and spatial distribution of annual NPP of terrestrial ecosystems in China for contemporary climate. Second, we applied TEM to quantify the equilibrium responses of annual NPP in China to changes in atmospheric CO_2 concentration and climate projected by three GCMs. We examined the TEM simulation results across the spatial scales of grid cell, biome and continent. The analysis will help us to understand how the abiotic factors (*e.g.*, climate, soil texture) control the magnitude and spatial distribution of NPP in China.

2. Model and Data

2.1 The Terrestrial Ecosystem Model (TEM)

The TEM (Figure 1) is a process-based ecosystem model that simulates important carbon and nitrogen fluxes and pools for various terrestrial biomes (Raich, *et al.,* 1991; McGuire, *et al.,* 1992, 1993, 1995). The TEM has been used to examine patterns of net primary production (NPP) in South America (Raich, *et al.,* 1991) and North America (McGuire, *et al.,* 1992) for contemporary climate. The model has also been used to estimate the responses of NPP of the terrestrial biosphere to climate change projected by four GCMs (Melillo, *et al.,* 1993). In this study, we use version 4.0 of TEM, which was modified from TEM version 3 to improve patterns of soil organic carbon storage along gradients of temperature, moisture and soil texture (McGuire, *et al.,* 1995, 1996). Version 4.0 of TEM has also been used to estimate the responses of NPP and carbon storage of terrestrial ecosystems to climate change in the conterminous United State (VEMAP Members, 1995; Pan, *et al.,* 1996a) and at the global scale (McGuire, *et al.,* 1996; Xiao, *et al.,* 1996a, 1996b). Detailed descriptions of TEM are documented in Raich, *et al.* (1991) and McGuire, *et al.* (1992). The recent TEM modifications are presented elsewhere (McGuire, *et al.,* 1995, 1996). To help understand how climate change and elevated CO_2 influence NPP in TEM, we review the key processes related to NPP.

Net primary production (NPP) is calculated as the difference between gross primary production (GPP) and plant respiration (R_A). The flux GPP is calculated at each monthly time step as follows:

$$GPP = C_{max}\, f(PAR)\, f(LEAF)\, f(T)\, f(CO_2, H_2O)\, f(NA) \quad (1)$$

where C_{max} is the maximum rate of C assimilation, PAR is photosynthetically active radiation, LEAF is leaf area relative to maximum annual leaf area, T is temperature, CO_2 is atmospheric CO_2 concentration, H_2O is water availability, and NA is nitrogen availability.

The effect of CO_2 and water availability on GPP are interrelated. The function $f(CO_2, H_2O)$ is described by the hyperbolic relationship:

$$f(CO_2, H_2O) = Ci / (kc + Ci) \quad (2)$$

where Ci is the concentration of CO_2 within leaves of the canopy and kc is the half-saturation constant for CO_2 uptake by plants. The relationship between CO_2 concentration inside stomatal cavities (Ci) and in the atmosphere (Ca) is directly proportional to relative moisture availability (Raich, *et al.,* 1991):

$$Ci = GvCa \quad (3a)$$
$$Gv = 0.1 + (0.9\ EET/PET) \quad (3b)$$

where Gv is unitless multiplier that accounts for changes in leaf conductivity to CO_2 resulting from changes in moisture availability, PET is potential evapotranspiration and EET is the estimated evapotranspiration. The flux PET is calculated as a function of mean air temperature and solar radiation (Jensen and Haise, 1963). The flux EET is equal to PET in wet months but is modeled as a function of rainfall, snowmelt recharge and a change of soil moisture in dry months (Vorosmarty, *et al.,* 1989).

The results from CO_2-enrichment studies indicate that the response of plant productivity to doubled CO_2 ranges from 20% to 50%, given adequate nutrients and water (Kimball, 1975; Gates, 1985). In TEM, the parameter kc (400 ppmv) has been chosen to increase $f(CO_2, H_2O)$ by 37% for a doubling of atmospheric CO_2 concentration from 340 ppmv to 680 ppmv, with canopy conductance equal to 1 (McGuire, *et al.,* 1992, 1993). It is important to note that the response of GPP to doubled CO_2 is not a constant 37% for kc of 400 ppmv, because GPP calculation is also affected by $f(NA)$, which represents the limiting effect of vegetation nitrogen status on GPP (McGuire, *et al.,* 1992, 1993; Melillo, *et al.,* 1993). Vegetation nitrogen status is determined by vegetation nitrogen uptake (NUPTAKE) and nitrogen from the labile nitrogen pool of vegetation (NMOBIL). The nitrogen down-regulation of GPP response to elevated CO_2 in TEM is discussed elsewhere (McGuire, *et al.,* 1996).

Increasing photosynthetically active radiation (PAR) increases GPP hyperbolically in the following form: $f(PAR) = PAR / (ki + PAR)$. A mean value of 314 J $cm^{-2}d^{-1}$ for ki from published leaf studies is used and applied to entire leaf canopies independent of vegetation types (Raich, *et al.,* 1991). Cloudiness affects the amount of solar irradiance, including PAR, that reaches the canopy of vegetation.

The effect of air temperature on GPP is described by allowing $f(T)$ to increase in a parabolic fashion to a grid-cell specific optimum temperature. Between the optimum temperature and a maximum vegetation-specific temperature constraint, $f(T)$ is equal to 1.0. Above the maximum

temperature constraint, *f*(T) declines rapidly to 0.0 (McGuire, *et al.,* 1996). Air temperature also affects plant respiration (R_A). The flux R_A includes both maintenance respiration (R_M) and construction respiration (R_C). The flux R_M increases logarithmically with temperature using a Q_{10} value that varies from 1.5 to 2.5 (McGuire, *et al.,* 1992). The flux R_C is determined to be 20% of the difference between GPP and R_M (Raich, *et al.,* 1991). Thus, changes in NPP are directly related to changes in CO_2, temperature, precipitation and cloudiness.

The simulation of TEM requires the use of soil- and vegetation-specific parameters appropriate to an ecosystem type. Although many of the vegetation-specific parameters in the model are defined from published references, some are determined by calibrating TEM to the fluxes and pool sizes of an intensively studied field site. Most of the data used to calibrate TEM for the 18 vegetation types of our global vegetation classification are documented elsewhere (Raich, *et al.,* 1991; McGuire, *et al.,* 1992, 1996).

2.2 Spatial data for extrapolation of TEM

The driving variables for the spatial extrapolation of TEM are vegetation types, elevation, soil texture, monthly mean temperature, monthly precipitation, monthly mean cloudiness, and several hydrological variables (potential evapotranspiration, estimated evapotranspiration and soil moisture). Hydrological inputs for TEM are generated by a water balance model (Vorosmarty, *et al.,* 1989) that uses the same climate, elevation, soils and vegetation data.

In this study, the spatial data used to drive TEM are derived from our global data sets (Melillo, *et al.,* 1993; McGuire, *et al.,* 1995, 1996; Xiao, *et al.,* 1996a), which are organized in a grid at a 0.5˚ (latitude) × 0.5˚ (longitude) resolution. China has 3,852 grid cells, including six grid cells of inland water body and 26 grid cells of wetlands. The TEM does not estimate NPP and carbon storage for grid cells defined as water or wetland ecosystems, so the extrapolation of TEM to China requires the application of TEM to 3820 grid cells.

We use potential vegetation in this study. Our global classification of potential vegetation includes 18 upland biomes (Melillo, *et al.,* 1993). In developing the global vegetation data, the Vegetation Map of China (Hou, *et al.,* 1982) was used in digitization and aggregation. There are 16 upland biomes in China (Plate 1). Forests dominate in southern China and eastern coastal areas, while arid and semi-arid biomes prevail in northwestern China. The Qinhai-Tibet plateau is dominated by polar desert/alpine tundra.

For elevation, we use the NCAR/NAVY global 10-minute dataset (NCAR/NAVY, 1984) aggregated to a 0.5˚ resolution. Elevation increases from east to west in China (Plate 2a). The Qinhai-Tibet plateau has the highest elevation, mostly over 3000 m. The Mongolia Plateau and Loess plateau have elevation of 1000–1500 m.

For soil texture data, we use the FAO/CSRC/MBL data set (FAO/CSRC/MBL, undated), which is a digitization version of the FAO-UNESCO World Soil Map (FAO/Unesco, 1971) at 0.5˚ grid resolution. There are seven texture classes in the FAO/CSRC/MBL data set that represents "average" soil profiles of the three FAO texture classes. Each FAO/CSRC/MBL soil texture class

defines a combination of sand, silt and clay proportions (Table 1). As shown in Plate 2b, soil texture is generally more coarse in northern China than in southern China.

For contemporary climate, we use the long-term average climate data from the global climate dataset of Cramer and Leemans (Wolfgang Cramer, personal communication), which is an update of an earlier version of global climate database (Leemans and Cramer,1990) that has monthly precipitation, temperature and sunshine duration. Monthly percent cloudiness is calculated as 100 percent minus monthly percent sunshine duration. On the continental scale, annual mean temperature is about 5.8 ˚C, annual precipitation is about 661 mm and annual mean cloudiness is 48%. Most precipitation occurs in the plant growing season (April to September). Geographically, annual mean temperature decreases gradually from south to north (Plate 2c). The Qinhai-Tibet Plateau has very low annual mean temperature, because of high elevation. Annual precipitation decreases from southeast to northwest, as affected by summer monsoon (Plate 2c). Vegetation distribution in China (Plate 1) is closely correlated to spatial patterns of temperature and precipitation (Plate 2). Characteristics of the climate variables for each of the 16 biomes are listed in Table 2. Tropical savanna has the highest annual mean temperature (24.2 ˚C) and annual precipitation (1793 mm), while alpine tundra has the lowest annual mean temperature (–4.1 ˚C), and desert has the smallest amount of annual precipitation (74 mm).

2.3 Scenarios of climate change and elevated CO_2

We first ran TEM for contemporary climate at 312.5 ppmv CO_2 as the baseline for comparison. We used 312.5 ppmv CO_2 because it is the average value of atmospheric CO_2 concentration for the $1 \times CO_2$ simulations used by the GCMs described in Melillo, *et al.,* (1993). To help separate the relative importance of elevated CO_2 and climate changes, we then ran TEM under (1) elevated CO_2 only, (2) climate change only, and (3) climate change plus elevated CO_2. For each of the four simulations, we ran TEM to steady state, therefore, its estimates of annual NPP apply only to mature, undisturbed vegetation and ecosystems. We have not considered the impacts of changes in land use and land cover on NPP in this study.

For climate change predictions, we used climate outputs for "current" ($1 \times CO_2$) and "doubled" ($2 \times CO_2$) simulations from three GCMs, *i.e.*, Geophysical Fluid Dynamic Laboratory (GFDL-q, Weatherald and Manabe, 1988), Goddard Institute for Space Studies (GISS, Hansen, *et al.*, 1983, 1984) and Oregon State University (OSU, Schlesinger and Zhao, 1989). These GCMs have very coarse spatial resolutions, *i.e.*, 10.0˚ (longitude) × 7.83˚ (latitude) for GISS, 7.5˚ × 4.44˚ for GFDL and 5.0˚ × 4.00˚ for OSU. In order to be consistent with the spatial resolution of the contemporary climate data, the outputs of the GCMs were interpolated to a 0.5˚ × 0.5˚ grid resolution by applying a spherical interpolation routine (Willmott, *et al.*, 1985) to the data.

We calculated the differences in monthly mean temperature and the ratios in monthly precipitation and mean monthly cloudiness between the $2 \times CO_2$ and $1 \times CO_2$ simulations of the GCMs. The OSU climate has the smallest changes in annual mean temperature and annual precipitation, while the GISS climate has the largest changes of annual mean temperature, annual

precipitation and annual mean cloudiness. The projected climate changes are the most uniform across China in the OSU climate, whereas the GISS climate has large spatial variations in the magnitude of projected climate changes (Plate 3). Spatial distributions of projected changes in annual mean temperature, annual precipitation and annual mean cloudiness vary among the GCMs (Plate 3).

The "current" ($1 \times CO_2$) climates simulated by GCMs differ considerably from the observed current climate. Therefore, in generating a "future climate," the differences in monthly mean temperature between the $2 \times CO_2$ and $1 \times CO_2$ simulations of a GCM are added to the contemporary monthly temperature data, and the ratios in monthly precipitation and cloudiness between the $2 \times CO_2$ and $1 \times CO_2$ simulations of a GCM are multiplied by the contemporary monthly precipitation and cloudiness data, respectively.

For elevated CO_2 level, we used an atmospheric CO_2 concentration of 519 ppmv, which corresponds to an effective CO_2 doubling for the radiative forcing, instead of using 625 ppmv CO_2 (Melillo, *et al.*, 1993). An "effective CO_2 doubling" has been defined as the combined radiative forcing of all greenhouse gases having the same radiative forcing as doubled CO_2 (Rosenzweig and Parry, 1994). According to recent studies, CO_2 will be the dominant long-lived greenhouse gas in the next century and its added radiative forcing contributes between 76% and 84% of the total additional radiative forcing (IPCC, 1995). Similar to another study (Xiao, *et al.*, 1996a), we assume that CO_2 contributes 76% of the total radiative forcing in this study, as projected by an economic-emission model, *i.e.*, Emission Prediction and Policy Analysis model (Prinn, *et al.*, 1996).

3. Net Primary Production Under Contemporary Climate at 312.5 ppmv CO_2

At the continental scale, TEM estimated that total annual NPP of terrestrial ecosystems in China for contemporary climate at 312.5 ppmv CO_2 is 3,653 TgC yr^{-1} (10^{12} gC yr^{-1}). Among the 16 biomes, annual NPP for a biome ranges from 4 TgC yr^{-1} in tropical savanna to 1,274 TgC yr^{-1} in temperate broadleaf evergreen forest (Table 3). Temperate forests (temperate coniferous forest, mixed forest, deciduous forest and broadleaf evergreen forest) account for 71.1% of the total annual NPP of China, but only cover about 35.6% of the total land area of China. Tropical forests (tropical deciduous forest and evergreen forest) occur over 4.7% of the total land area, and their annual NPP accounts for 9.1% of the total annual NPP of China. Arid and semi-arid ecosystems (desert, shrubland, shortgrassland and tallgrassland) occur over 28.5% of the total land area, but only account for 6.5% of the total annual NPP of China.

The relative importance of a biome to the total annual NPP of China reflects the relative productivity among biomes. Area-weighted mean biome NPP varies considerably among the 16 biomes (Table 3). Desert has the lowest mean biome NPP of 57 gC $m^{-2}yr^{-1}$. In desert and arid shrublands, NPP is controlled primarily by water availability, where annual precipitation is only 74 mm and 124 mm, respectively. In alpine desert/alpine tundra and wet/moist tundra, NPP is controlled primarily by low temperature, which results in a short plant growing season and low

nitrogen availability because of lower rate of net nitrogen (N) mineralization (NMIN). Temperate broadleaf evergreen forest is the most productive biome with a mean biome NPP of 890 gC $m^{-2}yr^{-1}$. In general, NMIN is higher in warm temperate and tropical biomes, but lower in high latitude and plateau biomes (Table 3). This indicates that mean biome NPP is closely related to annual net nitrogen mineralization rate in soils.

Spatial variation of NPP within a biome differs among the 16 biomes (Table 3). Desert has the largest spatial variation in NPP with a coefficient of variation of 63%. In contrast, tropical deciduous forest and evergreen forest have small spatial variations in NPP with a coefficient of variation of 10%. Spatial variation of NPP within a biome is primarily determined by spatial variations of climate. As shown in Table 2, spatial variations in temperature and precipitation within a biome are large and differ among the biomes. The coefficient of variation in annual precipitation is large in desert, xeromorphic forest and arid shrubland, but small in tropical forests (Table 2).

At the scale of grid cell, annual NPP is significantly correlated with annual precipitation (Figure 2), annual mean temperature (Figure 3) and annual mean cloudiness (Figure 4). Annual precipitation accounts for 60% of the total variation in annual NPP among the 3,820 pixels, annual mean temperature accounts for 52%, and annual mean cloudiness accounts for 52%, respectively. Annual precipitation (P_{ann}) and annual mean temperature (T_{ann}) together accounts for 70% of the total variation in annual NPP ($NPP = 54.0 + 0.35\ P_{ann} + 1.76\ T_{ann}$, $r^2 = 0.70$, $p < 0.001$). Annual precipitation, annual mean temperature and annual mean cloudiness (C_{ann}) together account for 72% of the total variation in annual NPP ($NPP = -127.1 + 0.26\ P_{ann} + 16.2\ T_{ann} + 5.2\ C_{ann}$, $r^2 = 0.72$, $p < 0.001$).

Geographically, annual NPP decreases from southeast to northwest (Plate 4a). Southern China has high annual NPP of more than 1,200 gC $m^{-2}yr^{-1}$. The spatial patterns of NPP are correlated with the spatial patterns of precipitation and temperature (Plate 3). Annual NPP in Qinhai-Tibet Plateau is very low because of low temperature and the short plant growing season. Annual NPP in Xinjian, Ninxia and Inner Mongolia is also very low, because of the small amount of annual precipitation.

4. Equilibrium Responses of Net Primary Production to Changes in Climate and CO_2

4.1 NPP response to climate change only

For climate change with 312.5 ppmv CO_2, TEM estimates that the continental response of annual NPP in China ranges from a decrease of 54.8 TgC yr^{-1} (–1.5%) for the GISS climate to an increase of 306.9 TgC yr^{-1} (8.4%) for the GFDL-q climate (Table 4). These differences in NPP response are determined by the differences among the three GCM climates. According to the GCMs projections, changes in annual mean temperature in China ranges from an increase of 2.9 ˚C for the OSU climate to an increase of 4.2 ˚C for the GISS climate (Table 5). Annual precipitation increases considerably but varies little among the GCMs, *i.e.* 15.5% for the GFDL-q

climate to 17.6% for the GISS climate (Table 5). However, annual mean cloudiness declines slightly, ranging from –0.2% for the OSU climate to –1.2% for the GFDL-q climate (Table 5).

In TEM, climate change affects NPP in a number of ways. Temperature change will affect plant photosynthesis. Elevated temperature will increase potential evapotranspiration (PET) and plant respiration. Higher PET will generally result in lower soil moisture, which enhances water stress of plants. Higher plant respiration and stronger water stress of plants may reduce NPP. Elevated temperature will enhance decomposition of soil organic matter, which releases more mineralized N available for plant uptake. Enhanced uptake of N by plants may increase NPP. An increase of precipitation may increase soil moisture and thus alleviate water stress of plant, and it also enhances decomposition of soil organic matter. A decrease of cloudiness will increase amount of total solar radiation and photosynthetic active radiation (PAR) that reaches the canopy of vegetation. Higher PAR may increase GPP and NPP. Higher total solar radiation will increase PET. As described earlier, higher PET may enhance water stress of plants, which leads to a decrease of GPP and NPP.

At the biome scale, the response of annual NPP varies substantially within a GCM (Table 4). For the GISS climate, biome NPP ranges from a decrease of 13.9% in temperate coniferous forest to an increase of 28.0% in polar desert/alpine tundra. The TEM estimates that annual NPP in tundra and boreal forest increase substantially for the three GCM climates, because all the GCMs project large increases of temperature and precipitation in these biomes (Table 5). Elevated temperature in tundra and boreal regions will significantly prolong the plant growing season and increase nutrient availability from enhanced decomposition of soil organic matter. Annual NPP for arid biomes (desert and arid shrubland) decreases moderately, except for arid shrubland in the GISS climate, in which there are large increases of annual precipitation and annual mean cloudiness (Table 5). Annual NPP of tropical deciduous forest and evergreen forest increases moderately for the OSU climate but declines for both the GISS and GFDL-q climate. These responses are attributable to the larger increases of annual precipitation and annual mean cloudiness as well as a smaller increase in annual mean temperature in the OSU climate (Table 5). The most significant differences in annual NPP response among the GCM climates occur in temperate broadleaf evergreen forest, *i.e.*, –135 TgC yr^{-1} (–10.6%) for the GISS climate, 96 TgC yr^{-1} (7.5%) for the OSU climate and 107 TgC yr^{-1} (8.4%) for the GFDL-q climate. These differences can be attributed to the substantial increase of annual mean temperature (4.8 ˚C), large decrease of annual mean cloudiness (–10.9%) and slight decrease of annual precipitation (–1.2%) in the GISS climate (Table 5). In contrast, both the GFDL-q and OSU project smaller increases in temperature and larger increases in precipitation (Table 5).

The response of NPP to climate change has large regional variations within a GCM climate (Plate 4b). For the GISS climate, NPP decreases substantially in Southern China but increase in Northeastern China. In Southern China, the GISS GCM predicts the largest increase of annual mean temperature and a decrease of annual precipitation and annual mean cloudiness (Plate 3). For the three GCMs climate, annual NPP decreases less than 20 gC $m^{-2}yr^{-1}$ in the arid and semi-arid regions in the Northwestern China, including the Loess Plateau. The Qinhai-Tibet Plateau has an

increase of annual NPP less than 40 gC $m^{-2}yr^{-1}$. However, the geographical distribution of NPP response in Southern China varies considerably among the GCM climates (Plate 4b). In the GISS and OSU climates, annual NPP decreases significantly in the Chendu Plain in the Shichuan Province, where is the most productive agricultural zone and the most dense settlement of human population. In contrast, annual NPP increases in the Chendu Plain for the GFDL climate.

4.2 NPP response to elevated CO_2 only

For contemporary climate with elevated CO_2 (519 ppmv), TEM estimated that annual NPP increases by 219 TgC yr^{-1} (6.0%) in China. In TEM, a direct effect of elevated atmospheric CO_2 level is to increase the intercellular CO_2 concentration within the canopy, which potentially increases GPP via a Michaelis-Menton (hyperbolic) function. Elevated atmospheric CO_2 level may also indirectly affect GPP by altering the carbon-nitrogen status of the vegetation increase effort toward nitrogen uptake; increased effort is generally realized only when GPP is limited more by carbon availability than by nitrogen availability (VEMAP Members, 1995).

At the biome scale, annual NPP increases for all of the 16 biomes (Table 4). The NPP responses vary substantially among biomes, ranging from an increase of 1.9% in tall grasslands to an increase of 30.2% in desert (Table 4). Biomes in the arid regions (desert, arid shrubland) have the largest percentage increase in annual NPP. This is attributed mostly to a significant increase of water use efficiency of plants in the arid regions, where water is the primary limiting factor on NPP. Temperate forests and boreal forests are generally limited by the availability of inorganic nitrogen in the soils, and as the result, their responses to elevated CO_2 is strongly constrained by nitrogen availability. Tropical savanna, xeromorphic forest, tropical deciduous forest and tropical evergreen forest have large increases of annual NPP in the range of 7.5% to 18.8%. In the tropical regions, annual NPP of ecosystems is generally not limited by nitrogen, because of high rates of net N mineralization resulting from high temperatures.

The geographical distribution of NPP responses to elevated CO_2 has distinct spatial patterns (Plate 4c). Annual NPP increase from about 20 gC $m^{-2}yr^{-1}$ to 300 gC $m^{-2}yr^{-1}$ in Southeastern China. Annual NPP in arid regions increases in the range of 20 to 40 gC $m^{-2}yr^{-1}$. In the Qinhai-Tibet Plateau, the response of annual NPP is within ±20 gC $m^{-2}yr^{-1}$ (Plate 4c). Annual NPP in the Qinhai-Tibet Plateau is primarily controlled by low temperature and constrained by low nutrient availability.

4.3 NPP response to changes in climate and CO_2

At the continental scale, annual NPP of China for climate change at 519 ppmv CO_2 increases substantially but varies little among the GCM climates, ranging from 683 TgC yr^{-1} (18.7%) for the GISS climate to 851 TgC yr^{-1} (23.3%) for the GFDL-q climate. Annual NPP increases considerably for all of the 16 biomes among the three GCM climates (Table 4). Dryland ecosystems (desert, arid shrubland) have the largest percentage increases in annual NPP (more than 30%). Annual NPP in tundra and boreal forest also increases substantially (more than 20%).

Although the percentage increases in annual NPP for temperate broadleaf evergreen forest are moderate, this biome accounts for the largest portion of the increase of annual NPP in China: 238.2 TgC yr^{-1} for the OSU climate, 179.6 TgC yr^{-1} for the GISS climate and 284.1 TgC yr^{-1} for the GFDL-q climate.

Geographically, the responses of annual NPP decrease from southeast to northwest within a GCM climate (Plate 4d). The spatial patterns of NPP responses are generally similar among the three GCM climates. Annual NPP has a slight increase (< 40 gC $m^{-2}yr^{-1}$) in the Qinhai-Tibet plateau and arid regions, a moderate increase (40 to 60 gC $m^{-2}yr^{-1}$) in grasslands, and a large increase (> 60 gC $m^{-2}yr^{-1}$) in forest regions (Plate 4d). Increases of annual NPP in forest regions are the largest in the GFDL-q climate, up to 200–300 gC $m^{-2}yr^{-1}$ in the southern China. For the GISS climate, NPP decreases in scattered areas of the Southern China (Plate 4). There are slight differences in both the magnitude and spatial distributions of NPP responses in the transitional zones between forests and grasslands among the three GCM climates (Plate 4).

It is important to note that at the continental scale, the response of NPP to climate change at 519 ppmv CO_2 is much larger than the sum of the NPP response to elevated CO_2 only and the NPP response to climate change only (Table 4). For the OSU climate, the sum of the NPP response for climate change at 315 ppmv CO_2 (7.5%) and the NPP response for contemporary climate at 519 ppmv CO_2 (6.0%) is much lower than the 20.0% NPP response for climate change at 519 ppmv CO_2; the difference is attributed to the interaction between climate change and elevated CO_2. Similarly, the interaction between climate change and elevated CO_2 contributes about 9.0% to the overall response of NPP to climate change at 519 ppmv CO_2 for the GFDL-q climate and 14.2% for the GISS climate. The interaction between elevated CO_2 and climate change is primarily caused by enhanced plant nitrogen uptake and increasing availability of mineralized nitrogen and carbon (CO_2) resources. These results show clearly that the interaction between elevated CO_2 and climate change contributes significantly to the overall equilibrium response of NPP to changes in climate and CO_2 (Table 4).

The relative role of the interaction between elevated CO_2 and climate change varies among the 16 biomes, ranging from a large role in arid biomes (*e.g.*, desert, arid shrubland) to a small role in alpine tundra (Table 4). The relative role of the interaction between elevated CO_2 and climate change also varies among the three GCMs climates (Table 4). This indicates that geographical distributions of climate changes projected by the GCMs affect the interaction between elevated CO_2 and climate change at larger spatial scales.

5. Discussion

There are numerous field measurements of plant biomass and NPP for various ecosystems in China, however, few studies have estimated the spatial distribution of NPP in China on large spatial scales. Zhang (1993) calculated annual NPP for 671 weather stations in China, using the Chikugo model (Uchijima and Seino, 1985). Fang, *et al.*, (1995) and Xiao, *et al.*, (1996) estimated annual NPP in China in 1990, using Normalized Difference Vegetation Index (NDVI)

derived from remote sensing data of NOAA AVHRR. In our study, the TEM-estimated annual NPP of all the terrestrial ecosystems in China under contemporary climate at 312.5 ppmv CO_2 is 3,653 TgC yr^{-1}, about 8% of global terrestrial NPP (see Melillo, *et al.,* 1993). Application of process-based ecosystem models such as TEM provides an important and useful tool to study spatial patterns and dynamics of NPP in China, although NPP estimates can be improved with the collection of additional field data and remote sensing data to further develop and validate ecosystem models.

The TEM results show that annual NPP in China has a large spatial variation. The geographical distribution of annual NPP in this study is similar to Zhang (1993) and Xiao, *et al.* (1996), characterized by a gradient of high NPP in southeastern China to low NPP in northwestern China. The spatial patterns of NPP are closely correlated to the spatial distributions of abiotic factors, particularly climate. This indicates that the spatial representation of contemporary climate and other abiotic factors used in extrapolation of TEM for China may affect estimates of NPP. In an earlier study that examines three alternative geo-referenced data sets of climate, solar radiation and soil texture in estimating NPP of the conterminous United States, Pan, *et al*. (1996a) found that NPP estimates of TEM are sensitive to variations in the input data, and the relative importance of climate, soil texture and solar radiation to NPP estimates differs among the vegetation types.

The spatial input data used in this study are from our global data base and need to be updated with the new data available in China. For instance, the climate data used in this study are the long-term average values of weather records from about 300 weather stations in China (W. Cramer, personal communication). Leemans and Cramer (1990) compiled weather record data mainly for the period of 1931–1960. Zhang (1993) calculated biotemperature and potential evapotranspiration using long-term average data from about 671 weather stations in China. Using more weather stations in the spatial interpolation will improve the spatial and temporal (seasonal) representations of contemporary climate.

Major soils in Xinjian, Qinhai-Tibet plateau and Inner Mongolia have generally about 40 to 70% of sand proportion in soil texture (Xiong and Li, 1987), which is higher than the 35 or 45% of sand proportion we used in this study to drive TEM (Plate 2). In arid and semi-arid regions, coarse texture soils, which allow deep infiltration of water, may have lower evaporation but higher transpiration rate than fine texture soils (Noy-Meir, 1973; Sala, *et al.,* 1988). Primary production is therefore higher in coarse texture soils than in fine texture soils in arid and semi-arid regions (Noy-Meir, 1973). In grasslands of the Central Plains of United States, aboveground production increases with coarser soil texture when annual precipitation is less than 370 mm, but decreases when annual precipitation is greater than 370 mm (Sala, *et al.,* 1988).

Therefore, to improve estimates of NPP in China, geographically referenced spatial data with better spatial-temporal representations are critically needed. Improved data set will allow ecosystem models such as TEM to make more realistic estimates of NPP for contemporary climate. As the contemporary climate data sets are also used in generating a “future climate” for impact analyses of climate change, improved contemporary climate data sets are likely to reduce the uncertainty in estimating responses of NPP in China to climate change.

The TEM results show that NPP of terrestrial ecosystems in China is sensitive to changes in atmospheric CO_2 concentration and climate as projected by the GCMs. These results are consistent with an earlier study (Xiao, *et al.,* 1995) that used the CENTURY ecosystem model (Parton, *et al.,* 1993) at individual sites and showed that NPP in grasslands of Inner Mongolia of China is sensitive to changes in climate and atmospheric CO_2 concentration. The TEM results also show that the magnitude and spatial distribution of NPP responses vary considerably among the GCMs projections. The largest uncertainty in the NPP response to climate change among the three GCM climates occurs in Southern China. The uncertainty in NPP responses is related to the uncertainty in the GCMs projections for future climate change.

There is a large uncertainty in the GCMs projections for future climate changes. A number of GCMs are available (Mitchell, *et al.,* 1990). Most GCMs project a similar range of global surface temperature increase, but they vary significantly in the spatial patterns of projected changes in temperature and precipitation. Zhang and Wang (1993) examined the simulation results for $1 \times CO_2$ and $2 \times CO_2$ scenarios from the Community Climate Model (CCM) at the National Center for Atmospheric Research (NCAR) of the United States. Annual mean temperature in China increases by 2.5–3.0 ˚C. There is a large spatial variation in changes of annual precipitation in China. In particular, the NCAR CCM predicts a considerable decrease (about 200 mm) of annual precipitation in the semi-arid Loess Plateau, where serious soil-water erosion and land degradation occur extensively.

Because of the very coarse spatial resolutions of GCMs, GCMs are generally poor in representing regional climate change, especially in China, which has very complex topography and the climate is dominated by summer monsoon. Monsoon climate is characterized by seasonal jumps, large interannual variability and abrupt changes on decade and longer time scales. There are strong interactions between climate and ecosystems in the Asian monsoon region on various time scales (Fu, 1995a). For instance, the normalized difference vegetation index (NDVI) for southern China varied significantly in the period of 1985–1990 (Fu, 1995a). The coupling of GCMs and meso-scale climate models with detailed representations of topography and ecosystem dynamics may generate better spatial-temporal representations of climate change in China (Fu, 1995b).

In this study, we have not considered the responses of vegetation distribution to climate change and elevated CO_2. Climate change is likely to affect the spatial distribution of vegetation in China (Zhang and Liu, 1993; Zhang and Song, 1993; Zhang, 1993; Wang and Zhao, 1995; Zhou and Zhang, 1996). Vegetation redistribution can affect regional estimates of NPP of terrestrial ecosystems (VEMAP Members, 1995). How climate change and elevated CO_2 affect vegetation distribution in China and consequently NPP is discussed in another paper (Pan, *et al.,* 1996b).

We used the potential vegetation of China in this study. Thus, we have not considered the effects of land use and management on NPP in China. In the last several thousand years of agricultural practice, a large portion of uplands has been converted to croplands. According to the Vegetation Map of China (Hou, *et al.,* 1982), the area of croplands is approximately 1.5 million km^2, or about 15% of the total land area of China. Based on the Land Use Map of China at the scale of 1:1,000,000 (Wu, 1990), cultivated lands account for about 14.2% of the total land area of

China (Wu and Guo, 1994). Conversion of forests to croplands results in significant losses of NPP and carbon storage (Houghton and Skole, 1990). Climate change is likely to have significant impacts on physical geographical zones (Zhao, 1993) and agriculture in China (Wang, 1993; Gong and Hameed, 1993; Ohta, *et al.*, 1995). This study provides a baseline for future studies to investigate the impacts of changes in land use and land cover on NPP and carbon storage of China.

In summary, this study demonstrates the usefulness of integrating a process-based ecosystem model with geo-referenced spatial data in China for examining the spatial patterns and dynamics of net primary production of terrestrial ecosystems. However, the analyses in this study are based on an equilibrium changes in climate and carbon fluxes of terrestrial ecosystems. The time course of changes in atmospheric CO_2 concentration, climate, land use and anthropogenic nitrogen deposition from the last several centuries to next century have not been considered. We are beginning to conduct transient simulations of TEM to track the path and magnitude of the responses of NPP over time (Melillo, *et al.*, 1996), but progress is hindered by a lack of both historical and future data with better spatial-temporal representation on climate, land use and N deposition in China. As these data sets become available in the near future, we should be able to improve the estimates of NPP and to better assess the effects of land use and climate changes on NPP of terrestrial ecosystems in China.

Acknowledgments

The study was supported by the National Aeronautics and Space Administration's Earth Observing System (NAGW-2669), the Department of Energy's National Institute for Global Environmental Change (No: 901214-HAR) and the Joint Program on Science and Policy of Global Change at the Massachusetts Institute of Technology (CE-S-462041).

References

Fang, Z., Q. Xiao, Y. Liu and R. Sheng, 1995, Monitoring of some surface properties in China by NOAA AVHRR. *In:* "China Contributions to Global Change Studies," D. Yu and H. Lin (eds.), Science Press, Beijing, p. 146–151.

FAO/CSRC/MBL (undated), Soil Map of the World, 1:5,000,000, Unesco, Paris, France. Digitization (0.5˚ resolution) by Complex Systems Research Center, University of New Hampshire, Durham, and modifications by Marine Biological Laboratory, Woods Hole, MA.

FAO/UNESCO, 1971, Soil Map of the World, 1:5,000,000, Unesco, Paris, France.

Fu, C., 1995a, Dynamics of monsoon-driven ecosystem: Concept, preliminary evidence and proposal for further research. *In*: "China Contributions to Global Change Studies," D. Yu and H. Lin (eds.), Science Press, Beijing, p. 103–106.

Fu, C., 1995b, Simulation of summer monsoon in east China by high resolution regional climate-ecosystem model (RCEM), *In:* "China Contributions to Global Change Studies," D. Yu and H. Lin (eds.), Science Press, Beijing, p. 142–145.

Gates, D.M., 1985, Global biospheric response to increasing atmospheric carbon dioxide concentration. *In:* "Direct Effect of Increasing Carbon Dioxide on Vegetation," B.R. Strain and J.D. Cure (eds.), DOE/ER-0238, United States Department of Energy, Washington D.C.,

p. 171–184.

Gong, G., and S. Hameed, 1993, Identification of climatically sensitive agricultural zones of China. *In:* "Climate Change and Its Impact," Y. Zhang, P. Zhang, H. Zhang and Z. Lin (eds.), Meteorology Press, Beijing, p. 78–90. (in Chinese with English abstract)

Hansen, J., G. Russel, D. Rind, P. Stone, A. Lacis, S. Lebedeff, R. Ruedy and L. Travis, 1983, Efficient three dimensional global models for climate studies: Model I and II, *Monthly Weather Review*, **111**:609–662.

Hansen, J., A. Lacis, D. Rind, G. Russel, P. Stone, I. Fung, R. Ruedy and J. Lerner, 1984, Climate sensitivity: Analysis of feedback mechanisms. *In:* "Climate process and Climate Sensitivity," J.E. Hansen and T. Takahashi (eds.), Geophysical Monograph 29, Maurice Ewing series 5, American Geophysical Union, Washington, D.C., p. 130–163.

Hou, X. (ed.), 1982, Vegetation map of China, 2nd edition, Science Press, Beijing. (in Chinese)

Houghton, R.A., and D.L. Skole, 1990, Changes in the global carbon cycle between 1700 and 1985. *In:* "The Earth as Transformed by Human Action," B.L. Turner, et al. (eds.), Cambridge University Press, Cambridge, UK, p. 393–408.

IPCC (Intergovernmental Panel on Climate Change), 1995, *Climate Change 1994: Radiative forcing of climate change and an evaluation of the IPCC IS92 emission scenarios*, Cambridge University Press, New York, p. 196–197.

Jensen, M.E., and H.E. Haise, 1963, Estimating evapotranspiration from solar radiation, *Journal of the Irrigation and Drainage Division*, **4**:15–41.

Kimball, B.A., 1975, Carbon dioxide and agricultural yield: An assemblage and analysis of 430 prior observations, *Agronomy Journal*, **75**:779–788.

Leemans, R., and W. P. Cramer, 1990, The IIASA climate database for land areas on a grid with 0.5˚ resolution, WP-90-41, International Institute for Applied Systems Analysis, Laxenburg, Austria, 60 pp.

Manabe, S., and R.T. Wetherald, 1987, Large scale changes in soil wetness induced by an increase in carbon dioxide, *Journal of the Atmospheric Sciences*, **44**:1211–1235.

McGuire, A.D., J.M. Melillo, D.W. Kicklighter, Y. Pan, X. Xiao, J. Helfrich, B. Moore, III, C.J. Vorosmarty and A.L. Schloss, 1996, The role of the nitrogen cycle in the global response of net primary production and carbon storage to doubled atmospheric carbon dioxide, *Global Biogeochemical Cycles* (in review).

McGuire, A.D., J.M. Melillo, D.W. Kicklighter and L.A. Joyce, 1995, Equilibrium response of soil organic carbon to climate change: empirical and process-based estimates, *Journal of Biogeography*, **22**:785–796.

McGuire, A.D., L.A. Joyce, D.W. Kicklighter, J.M. Melillo, G. Esser and C.J. Vorosmarty, 1993, Productivity response of climax temperate forests to elevated temperature and carbon dioxide: A North America comparison between two global models, *Climatic Change*, **24**:287-310.

McGuire, A.D., J.M. Melillo, L.A. Joyce, D.W. Kicklighter, A.L. Grace, B. Moore, III and C.J. Vorosmarty, 1992, Interactions between carbon and nitrogen dynamics in estimating net primary productivity for potential vegetation in North America, *Global Biogeochemical Cycles*, **6**(2):101–124.

Melillo, J.M., I.C. Prentice, G.D. Farquhar, E.D. Schulze and O.E.Sala, 1996, Terrestrial biotic responses to environmental change and feedback to climate. *In:* "IPCC Climate Change 1995: The Science of Climate Change," Intergovernmental Panel on Climate Change, Cambridge University Press, p. 445–481.

Melillo, J.M., 1994, Modeling land-atmospheric interaction: A short review. *In:* "Changes in Land Use and Land Cover: A Global Perspective," W.B. Meyer and B.L. Turner (eds.), Cambridge University Press, p. 387–409.

Melillo, J.M., A.D. McGuire, D.W. Kicklighter, B. Moore, III, C.J. Vorosmarty and A.L. Schloss, 1993, Global climate change and terrestrial net primary production, *Nature*, **363**:234–240.

Mitchell, J.F.B., S. Manabe, V. Meleshko and T. Tokioka, 1990, Equilibrium climate change and its implications for the future. *In:* "Climate Change: The IPCC Scientific Assessment," J.T. Houghton, G.J. Jenkins and J.J. Ephraums (eds.), Cambridge University Press, New York, p. 131–172.

NCAR/Navy, 1984, Global 10-minute elevation data. Digital tape available through National Oceanic and Atmospheric Administration, National Geophysical Data Center, Boulder, CO.

Noy-Meir, I., 1973, Desert ecosystems: Environment and producers, *Annual Review of Ecology and Systematic*, **4**:25–51.

Ohta, S., Z. Uchijima and W. Oshima, 1995, Effect of $2 \times CO_2$ climatic warming on water temperature and agricultural potential in China, *Journal of Biogeography*, **22**:649–655.

Pan, Y., A.D. McGuire, D.W. Kicklighter and J.M. Melillo, 1996a, The importance of climate and soils on estimates of net primary production: A sensitivity analysis with the Terrestrial Ecosystem Model, *Global Change Biology*, **2**:5–23.

Pan, Y., J.M. Melillo, D.W. Kicklighter, X. Xiao and A.D. McGuire, 1996b, Potential response of net primary production in terrestrial ecosystems of China to climate change: A simulation study by Terrestrial Ecosystem Model coupled with vegetation redistribution, *Journal of Biogeography* (in preparation).

Parton, W.J., J.M.O. Scurlock, D.S. Ojima, T.G. Gilmanov, R.J. Scholes, Schimel, T.ÊKirchner, J.C. Menaut, T. Seastedt, T. Garcia Moya, A. Kamnalrut and J.I. Kinyamario, 1993, Observation and modeling of biomass and soil organic matter dynamics for the grassland biome worldwide, *Global Biogeochemical Cycles*, **7**(4):785–809.

Prinn, R., H. Jacoby, A. Sokolov, C. Wang, X. Xiao, Z. Yang, R. Eckaus, P. Stone, D.ÊEllerman, J. Melillo, J. Fitzmaurice, D. Kicklighter, Y. Liu and G. Holian, 1996, Integrated global system model for climate policy analysis: I. Model framework and sensitivity studies, Joint Program on the Science and Policy of Global Change, *Report No. 7*, Massachusetts Institute of Technology, Cambridge, MA, 76 pp.

Raich, J., W., E.B. Rastetter, J.M. Melillo, D.W. Kicklighter, P.A. Steudler, B.J. Peterson, A.L. Grace, B. Moore, III and C.J. Vorosmarty, 1991, Potential net primary productivity in south America: Application of a global model, *Ecological Applications*, **1**(4):399–429.

Sala, O.E., W.J. Parton, L.A. Joyce and W.K. Lauenroth, 1988, Primary production of the central grasslands region of the United States, *Ecology*, **69**:40–45.

Uchijima, Z., and H. Seino, 1985, Agroclimatic evaluation of net primary productivity of natural vegetations: (1) Chikugo model for evaluating net primary productivity, *Journal of Agricultural Meteorology*, **40**(4):343–352.

VEMAP Members, 1995, Vegetation/Ecosystem modeling and analysis project: Comparing biogeography and biogeochemistry models in a continental-scale study of terrestrial ecosystem responses to climate change and CO_2 doubling, *Global Biogeochemical Cycles*, **9**(4):407–437.

Vorosmarty, C.J., B. Moore, III, A.L. Grace, M.P. Gildea, J.M. Melillo, B.J. Peterson, E.B. Rastetter and P.A. Steudler, 1989, Continental scale models of water balance and fluvial transport: an application to South America, *Global Biogeochemical Cycles*, **3**(3):241–265.

Wang, B., 1993, How to deal with the problem of global warming. *In:* "Climate Change and Its Impact," Y. Zhang, P. Zhang, H. Zhang and Z. Lin (eds.), Meteorology Press, Beijing, p. 1-15. (in Chinese with English abstract)

Wang, F., and Z. Zhao, 1995, Impact of climate change on natural vegetation in China and its implication for agriculture, *Journal of Biogeography*, **22**:657–664.

Wang, W., and Y. Zhang, 1993, The potential change of precipitation of China under the

condition of globe warming induced by CO_2 doubling. *In:* "Climate Change and Its Impact," Y. Zhang, P. Zhang, H. Zhang and Z. Lin (eds.), Meteorology Press, Beijing, p. 257–265. (in Chinese with English abstract)

Wetherald, R.T., and S. Manabe, 1988, Cloud feedback processes in a general circulation model, *Journal of the Atmospheric Sciences*, **45**:1397–1415.

Willmott, C.J., M.R. Clinton and W.D. Philpot, 1985, Small-scale climate maps: A sensitivity analysis of some common assumptions associated with grid-point interpolation and contouring, *The American Cartographer*, **12**:5–16.

Wilson, C.A., and J.F.B. Mitchell, 1987, A doubled CO_2 climate sensitivity experiment with a global climate model including a simple ocean, *J. Geophysical Res.*, **92**(D11):13,315–13,343.

Wu, C., 1990, *Land Use Map of China* (1:1,000,000), Science Press, Beijing. (in Chinese)

Wu, C., and H. Guo, 1994, *Land Use of China*, Science Press, Beijing, p. 90. (in Chinese)

Xiao, X., D.S. Ojima, W.J. Parton, Z. Chen and D. Chen, 1995, Sensitivity of Inner Mongolia grasslands to global climate change, *Journal of Biogeography*, **22**:643–648.

Xiao, X., D.W. Kicklighter, J.M. Melillo, A.D. McGuire, P.H. Stone and A.P. Sokolov, 1996a, Linking a global terrestrial biogeochemistry model and a 2-dimensional climate model: Implications for the global carbon budget, *Tellus* (in press).

Xiao, X., J.M. Melillo, D.W. Kicklighter, A.D. McGuire, P.H. Stone and A.P. Sokolov, 1996b, The relative roles of changes in CO_2 and climate to the equilibrium responses of net primary production and carbon storage of the terrestrial biosphere, *Global Change Biology* (in review).

Xiao, Q., W. Chen, Y. Sheng and L. Guo, 1996, Estimating the net primary productivity in China using meteorological satellite data, *Acta Botanica Sinica*, **38**(1):35–39. (in Chinese with English abstract)

Xiong, Y., and Q. Li (eds.), 1987, *Soils of China*, Science Press, Beijing, p. 333. (in Chinese)

Zhang, X., 1993, A vegetation-climate classification system for global change studies in China, *Quaternary Sciences*, **2**:157–169. (in Chinese with English abstract)

Zhang, Y., and L. Liu, 1993, The potential impact of climate change on vegetation distribution in Northwest China. *In:* "Climate Change and Its Impact," Y. Zhang, P. Zhang, H. Zhang and Z. Lin (eds.), Meteorology Press, Beijing, p. 178–193. (in Chinese with English abstract)

Zhang, Y., and J. Song, 1993, The potential impact of climate change on the vegetation in the Northeast China, *ibid*, p. 194–204.

Zhang, Y., and W. Wang, 1993, The potential change of ground surface air temperature under the condition of global warming induced by CO_2 doubling, *ibid*, p. 248–255.

Zhao, M., 1993, Impact of climate change on physical geographical zones of China, *ibid*, p. 168-177.

Zhou, G., and X. Zhang, 1996, Study on climate-vegetation classification for global change in China, Acta Botanica Sinica, 38(1):8–17. (in Chinese with English abstract)

Tables, Figures and Color Plates

Table 1. Proportions of sand, silt and clay assigned to the FAO/CSRC/MBL soil texture class.

FAO/CSRC/MBL code	Combination of FAO codes[†]	Class description	% sand	% silt	% clay
1	1 (coarse textured)	sand	80	10	10
2	2 (medium textured)	loam	45	40	15
3	3 (fine textured)	clay	25	30	45
4	1 and 3 (coarse & fine)	sandy loam	65	20	15
5	1 and 2 (coarse & medium)	loam	45	40	15
6	2 and 3 (medium & fine)	clay loam	35	30	35
7	1, 2, and 3	loam	45	40	15
8	none assigned to lithosols	lithosols	45	40	15

[†] FAO codes: 1, coarse textured; 2, medium textured; 3, fine textured. No texture was assigned to lithosols. From Pan, *et al.*, 1996.

Table 2. Means, standard deviations and coefficient of variations (CV) of annual mean temperature, annual precipitation and annual mean cloudines in contemporary climate.

	# of grid	area	temperature (°C)			precipitation (mm)			cloudiness (%)		
Vegetation type	points	(10^3 km^2)	mean	stddev	CV (%)	mean	stddev	CV (%)	mean	stddev	CV (%)
Polar desert/alpine tundra	615	1,568	-4.1	2.7	-66	480	316	66	43	5	11
Wet/moist tundra	230	588	-2.4	2.9	-121	483	294	61	47	6	13
Boreal forest	141	319	-0.3	5	-1667	643	278	43	52	7	14
Temperate coniferous forest	99	274	13.2	4.7	36	1,249	384	31	63	6	10
Desert	132	315	8.6	2.4	28	74	62	85	36	4	11
Arid shrubland	537	1,251	6	3	50	124	106	86	37	5	12
Short grassland	281	647	2.4	2.7	113	311	156	50	39	6	15
Tall grassland	213	481	2.9	3.5	121	416	97	23	41	8	20
Temperate savanna	106	229	3	2.2	73	550	141	26	40	5	12
Temperate mixed forest	341	847	10.7	4.3	40	810	277	34	50	9	17
Temperate deciduous forest	346	810	5.8	5.1	88	735	238	32	49	11	23
Temperate broadleaf evergreen forest	524	1,432	14.7	2.6	18	1,320	269	20	69	6	9
Tropical savanna	2	6	24.2	0.7	3	1,793	18	1	48	3	7
Xeromorphic forest	96	223	6	3.2	53	243	167	69	36	4	11
Tropical deciduous forest	14	40	19.7	3.3	17	1,350	341	25	57	7	12
Tropical evergreen forest	143	406	19.4	3.7	19	1,590	374	23	61	7	11
TOTAL	3,820	9,437	5.8	7.6	131	661	493	75	48	13	26

Table 3. Estimates of annual net primary production and net nitrogen mineralization for contemporary climate at 312.5 ppmv CO_2.

Vegetation type	# of grid points	area (10^3 km^2)	Total NPP (TgC/yr)	NPP (gC/m^{2}yr) mean	stddev	max	min	CV (%)	NMIN (mgN/m^{2}yr) mean	stddev
Polar desert/alpine tundra	615	1,568	97	62	16	117	0	26	479	118
Wet/moist tundra	230	588	69	117	35	216	0	30	797	228
Boreal forest	141	319	82	256	72	489	52	28	2,666	741
Temperate coniferous forest	99	274	170	621	134	854	257	22	4,882	1,058
Desert	132	315	18	57	36	161	1	63	1,413	867
Arid shrubland	537	1,251	105	84	39	194	0	46	2,074	935
Short grassland	281	647	124	192	46	397	34	24	3,250	696
Tall grassland	213	481	113	235	51	376	139	22	3,630	578
Temperate savanna	106	229	110	482	69	858	306	14	6,116	660
Temperate mixed forest	341	847	528	623	106	992	303	17	6,559	1,229
Temperate deciduous forest	346	810	579	715	102	1,036	502	14	8,800	1,253
Temperate broadleaf evergreen forest	524	1,432	1,274	890	126	1,145	59	14	11,036	1,686
Tropical savanna	2	6	4	764	18	777	751	2	13,917	36
Xeromorphic forest	96	223	46	208	126	441	13	61	5,289	3,199
Tropical deciduous forest	14	40	31	771	75	879	652	10	17,267	1,511
Tropical evergreen forest	143	406	302	744	74	935	356	10	16,726	1,588
TOTAL	3,820	9,437	3,653	387	325	1,145	0	84	5,185	4,474

Table 4. Estimates of annual net primary production for climate at 312.5 ppmv CO_2 and its responses to elevated CO_2 and climate changes estimated by GCMs.

	312.5 ppmv CO_2				519 ppmv CO_2				interation between elevated CO_2 and climate change		
Vegetation type	Contemp† (TgC/yr)	OSU (%)	GISS (%)	GFDL-q (%)	Contemp† (%)	OSU (%)	GISS (%)	GFDL-q (%)	OSU (%)	GISS (%)	GFDL-q (%)
Polar desert/alpine tundra	97	21.5	28.0	29.6	2.6	25.9	33.7	35.0	1.8	3.0	2.8
Wet/moist tundra	69	20.4	22.5	29.3	4.0	27.1	30.1	34.8	2.8	3.7	1.5
Boreal forest	82	14.7	12.6	15.8	2.7	121.0	22.2	23.9	3.6	6.9	5.5
Temperate coniferous forest	170	2.7	-13.9	-0.8	7.6	20.7	7.3	17.2	10.4	13.5	10.4
Desert	18	-6.3	-2.4	-13.8	30.2	39.7	40.9	29.8	15.8	13.2	13.4
Arid shrubland	105	-5.8	0.7	-6.6	24.4	33.2	40.5	33.8	14.6	15.5	16.1
Short grassland	124	15.0	19.9	22.7	2.0	20.2	25.7	28.6	3.2	3.7	3.9
Tall grassland	113	11.3	19.1	20.8	1.9	15.5	22.7	23.9	2.3	1.8	1.2
Temperate savanna	110	5.3	9.3	4.7	3.4	13.6	18.3	20.7	4.9	5.7	12.6
Temperate mixed forest	528	4.7	-3.2	1.5	7.6	20.6	20.5	23.5	8.4	16.2	14.5
Temperate deciduous forest	579	10.7	7.7	12.7	3.6	19.2	20.5	24.2	5.0	9.2	8.0
Temperate broadleaf evergreen f.	1,274	7.4	-10.6	10.0	4.9	18.7	14.1	22.3	6.4	19.7	7.4
Tropical savanna	4	3.7	-3.3	-6.6	11.1	27.2	18.4	12.8	12.3	10.5	8.2
Xeromorphic forest	46	-6.3	-1.3	-5.4	18.8	24.9	29.9	28.3	12.4	12.5	15.0
Tropical deciduous forest	31	5.7	-9.2	-4.1	9.0	21.9	15.8	15.8	7.2	16.0	10.9
Tropical evergreen forest	302	3.9	-9.7	-2.3	7.5	19.3	14.8	16.9	7.9	17.0	11.7
TOTAL	3,653	7.5	-1.5	8.4	6.0	20.0	18.7	23.3	6.6	14.2	9.0

† Contemporary climate

Note: for each vegetation type the number of grid points and area are as shown above in Table 3 (columns 1 and 2).

Table 5. Means of changes in annual mean temperature (T), annual precipiation (P), and annual mean cloudiness (C), projected by GCMs.

Vegetation type	# of grid points	area (10^3 km^2)	GISS T (˚C)	GISS P (%)	GISS C (%)	GFDL-q T (˚C)	GFDL-q P (%)	GFDL-q C (%)	OSU T (˚C)	OSU P (%)	OSU C (%)
Polar desert/alpine tundra	615	1,568	4.3	35.4	5.3	3.9	18.7	0.2	3.1	14.5	-1.9
Wet/moist tundra	230	588	4	25.3	2.3	3.7	24.7	3	3.1	13.4	-1.7
Boreal forest	141	319	4.1	11.5	-1.5	4.2	21.3	1.6	3.1	12.2	-1.4
Temperate coniferous forest	99	274	4.6	-3.7	-9	3.6	10.2	-3.7	2.7	28.8	5.6
Desert	132	315	4.4	25.7	3.8	4.2	8.1	-5.7	2.9	15.1	-1.4
Arid shrubland	537	1,251	4.2	25.5	3.4	4.4	9.3	-4.5	2.9	11.7	-1.7
Short grassland	281	647	4	15.1	-0.8	4.4	13.5	-2.6	2.9	9.3	-2.3
Tall grassland	213	481	3.8	16.3	-1.3	4.6	16	-0.7	2.9	6	-3.3
Temperate savanna	106	229	3.8	9.6	-1.9	5	16.6	-0.2	2.9	5.3	-3.3
Temperate mixed forest	341	847	4	18.9	-2.2	4.4	18.6	2	2.8	12.4	-2.4
Temperate deciduous forest	346	810	4	13	-3.2	4.5	21.4	2.3	2.8	10.3	-2.5
Temperate broadleaf evergreen forest	524	1,432	4.8	-1.2	-10.9	3.9	15.4	-0.6	2.5	30.6	5.3
Tropical savanna	2	6	3.4	24.4	4.8	3.1	0.6	-5.9	2.1	34.8	16.2
Xeromorphic forest	96	223	4	18.8	0.1	4.4	13.6	-3.3	2.9	9.4	-2.7
Tropical deciduous forest	14	40	4.1	10.6	-1.1	3.3	-4.8	-10.8	2.4	40.3	14.5
Tropical evergreen forest	143	406	4	8.8	-4.6	3.5	1.7	-6.2	2.4	36.9	10.4
TOTAL	3,820	9,437	4.2	17.6	-1.2	4.1	15.5	-1	2.9	16.3	-0.2

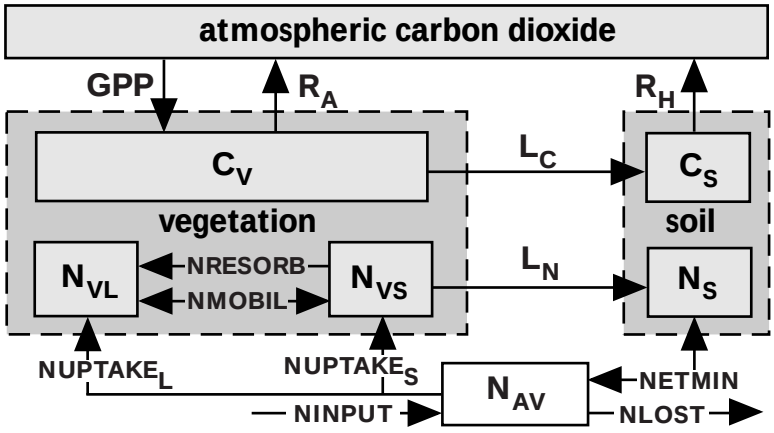

Figure 1. The Terrestrial Ecosystem Model (TEM). The state variables are: carbon in vegetation (C_V); structural nitrogen in vegetation (N_{VS}); labile nitrogen in vegetation (N_{VL}); organic carbon in soils and detritus (C_S); organic nitrogen in soils and detritus (N_S); and available soil inorganic nitrogen (N_{AV}). Arrows show carbon and nitrogen fluxes: GPP, gross primary productivity; RA, autotrophic respiration; R_H, heterotrophic respiration; L_C, litterfall carbon; L_N, litterfall nitrogen; $NUPTAKE_S$, N uptake into the structural N pool of the vegetation; $NUPTAKE_L$, N uptake into the labile N pool of the vegetation; NRESORB, N resorption from dying tissue into the labile N pool of the vegetation; NMOBIL, N mobilized between the structural and labile N pools of the vegetation; NETNMIN, net N mineralization of soil organic N; NINPUT, N inputs from the outside of the ecosystem; and NLOST, N loss from the ecosystem.